Additive noise properties of active matrix flat-panel imagers

M. Maolinbay,[a] Y. El-Mohri, L. E. Antonuk, K.-W. Jee,
S. Nassif, X. Rong,[b] and Q. Zhao
Department of Radiation Oncology, University of Michigan Medical Center, Ann Arbor, Michigan 48109

(Received 21 October 1999; accepted for publication 17 May 2000)

A detailed theoretical and empirical investigation of additive noise for indirect detection, active matrix flat-panel imagers (AMFPIs) has been performed. Such imagers comprise a pixelated array, incorporating photodiodes and thin-film transistors (TFTs), and an associated electronic acquisition system. A theoretical model of additive noise, defined as the noise of an imaging system in the absence of radiation, has been developed. This model is based upon an equivalent-noise-circuit representation of an AMFPI. The model contains a number of uncorrelated noise components which have been designated as pixel noise, data line thermal noise, externally coupled noise, preamplifier noise and digitization noise. Pixel noise is further divided into the following components: TFT thermal noise, shot and $1/f$ noise associated with the TFT and photodiode leakage currents, and TFT transient noise. Measurements of various additive noise components were carried out on a prototype imaging system based on a 508 μm pitch, $26\times 26\,\mathrm{cm}^2$ array. Other measurements were performed in the absence of the array, involving discrete components connected to the preamplifier input. Overall, model predictions of total additive noise as well as of pixel, preamplifier, and data line thermal noise components were in agreement with results of their measured counterparts. For the imaging system examined, the model predicts that pixel noise is dominated by shot and $1/f$ noise components of the photodiode and TFT at frame times above $\sim$1 s. As frame time decreases, pixel noise is increasingly dominated by TFT thermal noise. Under these conditions, the reasonable degree of agreement observed between measurements and model predictions provides strong evidence that the role of TFT thermal noise has been properly incorporated into the model. Finally, the role of the resistance and capacitance of array data lines in the model was investigated using discrete component circuits at the preamplifier input. Measurements of preamplifier noise and data line thermal noise components as a function of input capacitance and resistance were found to be in reasonable agreement with model predictions. © *2000 American Association of Physicists in Medicine.* [S0094-2405(00)01408-5]

Key words: additive noise, active matrix flat-panel imager, amorphous silicon, thin-film transistors

I. INTRODUCTION

Active matrix flat-panel imagers (AMFPIs) represent a technology that has the potential of bringing x-ray imaging into the digital age for a variety of applications including portal imaging, radiography, fluoroscopy, and mammography.[1–6] Toward facilitating this goal, it is useful to acquire a detailed knowledge of the noise performance of such imagers as such information is crucial in understanding performance limitations. The noise performance of an imaging system is determined by a variety of factors including quantum noise, which corresponds to fluctuations in the number of incident x-ray quanta, and additive noise, which corresponds to system noise in the absence of radiation.[7] Detailed knowledge of system noise is particularly valuable during the initial development of a new technology, since it can aid in the challenging task of system performance optimization. In this context, the additive noise component is of particular interest. If additive noise becomes a dominant component of the overall system noise, image quality is seriously degraded. This effect can be directly quantified by means of the signal to noise ratio (SNR) as well as the detective quantum efficiency (DQE) of the system. DQE, which is defined as the square of the ratio of the SNR at the output of a system to that at the input of a system, is a widely accepted measure of imaging performance.[8] For optimum imaging performance, it is desirable that system noise be dominated by x-ray quantum noise. Under such conditions, the imaging system is said to be input-quantum-limited. Therefore, for a given x-ray imaging application, it is desirable to minimize additive noise so as to allow input-quantum-limited operation down to the lowest possible exposures.

In the case of applications involving large x-ray exposures, such as portal imaging, mammography, and radiography, the signal to noise ratio (SNR) and the DQE of flat-panel imaging systems are generally limited by quantum noise.[1,7,9] However in applications involving low exposures, such as fluoroscopy or low exposure radiography, the additive noise can become a limiting factor in determining system performance.[3,5,10] Under such conditions, minimizing additive noise is highly desirable and can be facilitated through an understanding of the various noise sources. Such an understanding can be achieved through both empirical measurements and theoretical modeling of these noise

TABLE I. Symbols, definitions, and typical values for the array and preamplifier designs incorporated in the imaging system used for the measurements.

Symbols	Definitions	Typical values
	Pixel format (data×gate), array size	512×512, 26×26 cm^2
	Pixel pitch, photodiode geometric area	508 μm, 0.223 mm^2
	TFT dimensions	11 μm×88 μm
C_{pd}	photodiode capacitance	~20 pF[a]
I_{pd}	Photodiode leakage current	~110 fA at −6 V bias[a]
I_{TFT}	TFT-off leakage current	~1 fA[a]
Q_{tran}	TFT switching transient charge	165 fC[a] (maximum)
R_{off}	TFT-off resistance	$\sim 10^{14}\ \Omega$
C_{data}	data line capacitance	~75 pF (estimate)
R_{data}	data line resistance	10.2 KΩ[a]
V_{on}	TFT-on voltage	Adjustable, typically +6 V
V_{off}	TFT-off voltage	Adjustable, typically −10 V
V_{bias}	Photodiode reverse-bias voltage	Adjustable, typically −6 V
τ_{pix}	$=R_{on}C_{pd}$, Pixel time constant	~30 μs (estimate)
$\tau_{TFT\text{-}on}$	TFT-on period	Adjustable, typically ~180 μs
$\tau_{TFT\text{-}off}$	TFT-off period	Adjustable
τ_{int}	Preamplifier charge integration time	Programmable, ~150 μs
τ_{frame}	Time to readout one frame of data	Adjustable, min. 1800 μs
C_{fb}	Preamplifier feedback (gain) capacitor	Programmable
C_{amp}	Preamplifier internal input capacitor	~20 pF (estimate)
A	Preamplifier open-loop voltage gain	≳10 000
f_0	Preamplifier signal bandwidth	Variable depending on preamplifier operational conditions
g_m	Preamplifier transconductance	8 mA/V

[a]Measured values.

sources. In the present study, a theoretical model of additive noise has been developed based upon an equivalent noise circuit for an imager comprising an array of pixels and its associated acquisition electronics.

The theoretical model used in this study was applied to an indirect-detection active matrix flat-panel imager employing an array of amorphous silicon (*a*-Si:H) thin-film transistors (TFTs) and photodiodes.[1] The model describes the various sources contributing to additive noise including: pixel noise, data line thermal noise, externally coupled noise (e.g., from power supplies), preamplifier noise, and digitization noise associated with the analog-to-digital converters. The pixel noise includes thermal noise associated with the TFT-on resistance (when the TFT is conducting) as well as shot noise and $1/f$ noise associated with both the photodiode and TFT leakage currents. In order to test the validity of the model, measurements of both the total additive noise and some individual noise components were performed in the absence of radiation using a previously developed active matrix flat-panel imager.[1]

II. METHODS AND MATERIALS

A. Operational description of the imaging system

The empirical investigation performed to examine the additive noise model involved the use of an indirect detection, active matrix flat-panel imager comprising an array coupled to a custom electronic acquisition system.[11] The array has a pixel format of 512×512 with a pixel-to-pixel pitch of 508 μm giving a total area of 26×26 cm^2.[1,12] Design specifications for the array, typical operational parameters used for the measurements, and related symbols are given in Table I. Each pixel consists of an *n-i-p* (*n*-type, intrinsic, *p*-type layers) photodiode coupled to a TFT. Figure 1(a) shows a top view microphotograph of a pixel. The pixel TFT acts as a switch which allows integration of the imaging signal in the capacitance of the photodiode (C_{pd}) as well as readout of this signal by the acquisition system. Array pixels are arranged in a regular two-dimensional matrix of rows and columns. For a given row, the gate contacts of the corresponding TFTs are connected to a common conductive trace (the gate line) which, in turn, is connected to a peripheral gate driver circuit. For a given column, the drain contacts of the corresponding TFTs are connected to a common conductive trace (the data line) which, in turn, is connected to an external charge-sensitive preamplifier circuit. During imaging, electron–hole pairs generated in the photodiode are collected by means of an electric field established across it by an externally applied reverse bias voltage, V_{bias}. As long as the gate lines are maintained at a negative voltage, V_{off}, the TFTs remain nonconducting and the imaging signal is collected in the photodiodes. Readout of the imaging signal is accomplished by applying a positive voltage, V_{on}, to the gate lines, typically one gate line at a time. The TFTs along the corresponding row are thereby made conducting, with each TFT having a resistance R_{on}. This allows the imaging signal for each pixel to be sampled by the preamplifier for the corresponding data line while simultaneously initializing the pixels. In this study, the voltages V_{on} and V_{off} were maintained at values of 6 V and −10 V, respectively.

The acquisition system incorporates low noise, application specific integrated circuit (ASIC) preamplifiers, 16-bit

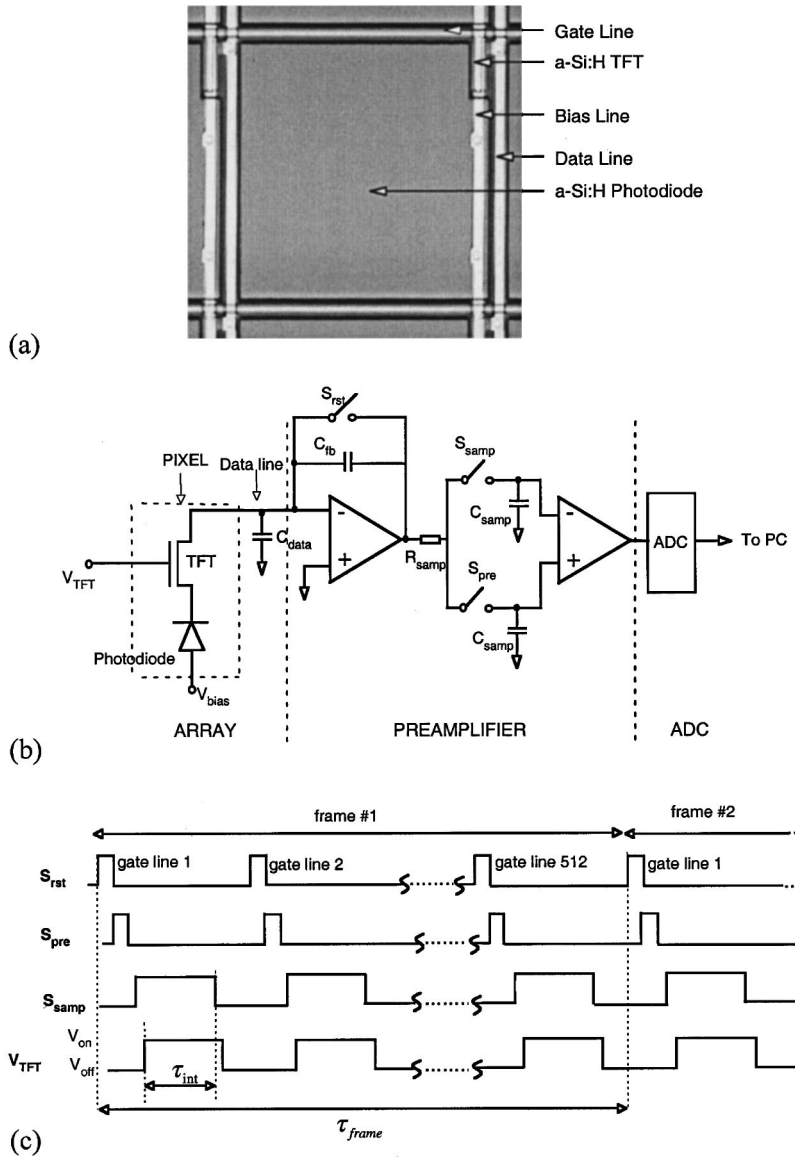

FIG. 1. (a) Microphotograph of an array pixel. (b) Schematic diagram of an array pixel (photodiode+TFT transistor) connected to a charge integrating preamplifier. The preamplifier has a programmable, bandwidth-limiting RC circuit ($R_{\text{samp}}C_{\text{samp}}$, where R_{samp} is variable). The preamplifier also has dual switches (presample, S_{pre}, and sample, S_{samp}) which are used for double sampling. An analog-to-digital converter (ADC) digitizes the preamplifier output. Also shown is the data-line capacitance, C_{data}. (c) Timing diagram illustrating the state of various switches shown in (b) as well as the gate line voltage, V_{TFT}, during readout of an array with 512 gate lines.

resolution analog-to-digital converters (ADCs), digital control logic and a host computer. The preamplifier is a 32-channel, charge integrating circuit offering double sampling as well as programmable bandwidth and gain settings.[13] Figure 1(b) shows the circuit diagram of a single array pixel and its corresponding preamplifier. Figure 1(c) shows a timing diagram for a typical acquisition sequence which can be summarized as follows. First, the reset switch, S_{rst}, is closed (for $\sim 5\ \mu$s) in order to initialize the preamplifier and to start the acquisition of a new row of pixel data. Immediately after, the presample switch, S_{pre}, is closed, allowing the circuit to perform an initial sampling of the preamplifier output (for $\sim 5\ \mu$s). This initial sample excludes any contribution from the pixel signal. Subsequently, a second sampling, which includes pixel signal, starts when the switch S_{samp} is closed. This action triggers the switching of the pixel TFT (V_{on}) thereby allowing the preamplifier to integrate the pixel signal. It also triggers an injection of charge into the preamp-

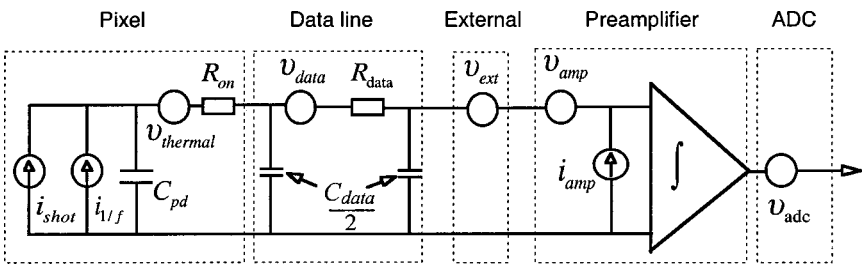

FIG. 2. Schematic illustration of a generalized additive noise model of a flat-panel imaging system. The model consists of five noise components: (a) pixel noise which includes TFT thermal noise, shot noise and $1/f$ noise; (b) data-line thermal noise; (c) externally coupled noise (e.g., from the power supplies); (d) preamplifier noise; and (e) digitization noise of the ADC. See main text for definition of symbols.

TABLE II. Summary of additive noise components for imaging systems of the type considered in this paper. All noise components are referred to the input of the preamplifier and represent RMS values.

Symbols	Noise components	Definitions and estimations	Comments
σ_{add}	Total additive noise	$=\sqrt{\sigma_{pix}^2+\sigma_{amp}^2+\sigma_{data}^2+\sigma_{ext}^2+\sigma_{dig}^2}$	Total additive noise of system
		$=\sqrt{\sigma_{pix}^2+\sigma_{base}^2}$	
σ_{pix}	Pixel noise	$=\sqrt{\sigma_{TFT\text{-}thermal}^2+\sigma_{tran}^2+\sigma_{pd\text{-}on}^2+\sigma_{pd\text{-}off}^2+\sigma_{TFT\text{-}off}^2}$	Becomes the dominant additive noise contribution for arrays with large pixels
$\sigma_{TFT\text{-}thermal}$	TFT thermal noise	$\approx\frac{1}{q}\sqrt{2kTC_{pd}}$	Applies for $f_0 \gg \frac{1}{2\pi\tau_{pix}}$
σ_{tran}	TFT transient noise	$\approx\sqrt{\frac{1}{q}Q_{tran}\left(1+\frac{f_L}{f^n}\right)}$ [a]	
$\sigma_{pd\text{-}off}$	Photodiode shot noise and $1/f$ noise with TFT off	$\approx\sqrt{\frac{1}{q}I_{pd\text{-}leak}\tau_{TFT\text{-}off}\left(1+\frac{f_L}{f^n}\right)}$ [a]	Becomes a dominant additive noise contribution only at very low frame rates (e.g., at ~0.1 fps)
$\sigma_{pd\text{-}on}$	Photodiode shot noise and $1/f$ noise with TFT on	$\approx\sqrt{\frac{1}{q}I_{pd\text{-}leak}\tau_{TFT\text{-}on}\left(1+\frac{f_L}{f^n}\right)}$ [a]	Negligible contribution due to short TFT-on time
$\sigma_{TFT\text{-}off}$	TFT shot noise and $1/f$ noise with TFT off	$\approx\sqrt{\frac{1}{q}I_{TFT\text{-}leak}\tau_{TFT\text{-}off}\left(1+\frac{f_L}{f^n}\right)}$ [a]	Negligible contribution due to small TFT leakage current
σ_{base}	Base system noise	$=\sqrt{\sigma_{amp}^2+\sigma_{data}^2+\sigma_{ext}^2+\sigma_{dig}^2}$	Additive noise excluding pixel noise
σ_{data}	Data line thermal noise	$=\frac{1}{q}C_{data}\sqrt{\pi kTR_{data}f_0}$	
σ_{amp}	Preamplifier noise	$=\frac{1}{q}(C_{data}+C_{amp})\sqrt{\frac{16\pi}{3}kT\frac{1}{g_m}f_0}$	
σ_{ext}	External noise	Externally coupled (correlated) noise	Depends on power supply, shielding, etc. Can be largely removed.
σ_{dig}	Digitization quantum noise	$=\frac{1}{q}\frac{Q_{signal}}{\sqrt{12}\times 2^{bits}}$ [b]	Not significant for high resolution ADCs

[a] f_L, empirical parameter, defines the corner frequency at which the $1/f$ noise becomes equal to the shot noise.
[b] Q_{signal}, maximum signal charge (in units of e^-) to be digitized; bits, effective resolution of the ADC (in units of ADC bits); n, spectral slope, determines the slope of $1/f$ noise spectral density.

lifier as an offset to compensate for a transient charge of opposite polarity caused by the TFT switching action.[2] The primary purpose of this correlated double sampling technique is to remove noise associated with the reset switch through subtraction of the two sampled signals. This technique, which is analogous to that used in charge coupled devices (CCDs), is routinely used in low-noise AMFPI acquisition systems.[14,15] The charge integration time, τ_{int}, of the preamplifier (which is defined as the period between the rising edge of V_{TFT} and the falling edge of S_{samp}) is typically set to be at least five times larger than the pixel time constant, τ_{pix} (given by $R_{on}C_{pd}$), so that the pixel signal is adequately sampled by the preamplifier. For most of the measurements, τ_{int} was kept constant at 150 μs. However, for some measurements, τ_{int} was varied from 5 to 150 μs in order to study noise as a function of this parameter.

The synchronized action between TFT switching and preamplifier charge integration is repeated until each row of pixels has been read out resulting in the acquisition of one frame of image data. The interval from the beginning of acquisition of a given image frame to the beginning of the next frame is defined as the frame time, τ_{frame}. In the present study, a wide range of frame times (1.8 ms up to ~50 s) was achieved through a combination of addressing only two gate lines per frame and by introducing a variable computer-controlled time delay between the acquisition of consecutive image frames. While the frame time for the majority of measurements was fixed at 1.8 ms (the minimum achievable) in order to minimize the noise contribution from the photodiode leakage current, some measurements were performed as a function of frame time.

B. Noise model

Figure 2 shows a generalized additive noise model of the imaging system shown in Fig. 1(b). In Fig. 2 the total additive noise is assumed to consist of five uncorrelated noise components: pixel noise, data line thermal noise, externally coupled noise, preamplifier noise, and ADC digitization noise. Each component has an equivalent noise source (de-

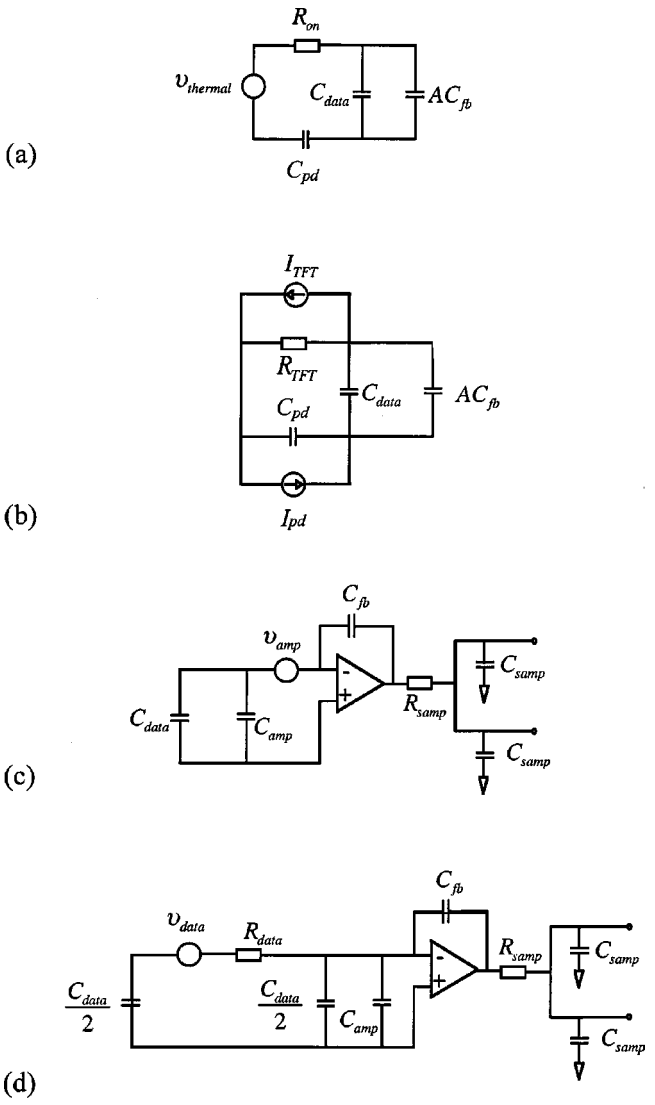

FIG. 3. (a) Equivalent circuit for the TFT thermal noise. The preamplifier input node is simplified to an equivalent capacitance, C_{in}^*, given by $C_{data}+AC_{fb}$. The symbols C_{pd}, C_{data}, and C_{fb} represent the photodiode, data line, and preamplifier feedback capacitance, respectively. The symbol A represents the open-loop voltage gain of the preamplifier. (b) Equivalent circuit for the shot noise and $1/f$ noise of the photodiode and of the TFT. The preamplifier input node is simplified to the equivalent capacitance, C_{in}^* as in (a). (c) Equivalent circuit for preamplifier noise. (d) Equivalent circuit for data line thermal noise.

noted by voltage density v or current density i) embedded in an interconnecting noise transfer network. Pixel noise consists of TFT thermal noise, shot noise and $1/f$ noise with noise densities $v_{thermal}$, i_{shot}, and $i_{1/f}$, respectively. The data line noise, with voltage noise density, v_{data}, consists of the thermal noise generated by the data line resistance, R_{data}. The externally coupled noise component, with voltage noise density v_{ext}, corresponds to all external noise which couples to the data lines through parasitic capacitance, including noise from the voltage supplies for V_{bias}, V_{off}, V_{on} and for the preamplifiers. The preamplifier noise is represented by an input voltage noise density, v_{amp}, in series, and a current noise density, i_{amp}, in parallel with the input of the preamplifier. ADC digitization noise is represented by a voltage noise density, v_{adc}. In this paper, because these noise sources are uncorrelated, they have been analyzed individually and the resulting noise charge, referred to the input of the preamplifier, has been estimated for each noise component. The total additive noise is then derived by summing all the noise components in quadrature. A summary of all additive noise components is given in Table II.

1. Pixel noise (σ_{pix})

Noise generating mechanisms within a pixel include random charge fluctuations induced by the thermal noise of the TFT-on resistance (R_{on}) (referred to as TFT thermal noise). These mechanisms also include shot and $1/f$ (flicker) noise induced by photodiode leakage currents, by TFT leakage currents, and by the TFT switching transient current.[2,16]

a. TFT thermal noise ($\sigma_{TFT\text{-}thermal}$): Figure 3(a) shows an equivalent noise circuit for a pixel connected to a preamplifier when the TFT is in the on state. (The TFT-off state is essentially an open circuit and the corresponding TFT thermal noise contribution is negligible.) The thermal noise spectral density, $v_{thermal}$, associated with the resistance R_{on} is expressed by the Johnson formula,[17]

$$\overline{v_{thermal}^2}=4kTR_{on}(\mathrm{V^2/Hz}), \tag{1}$$

where k is the Boltzmann constant and T is the absolute temperature. This expression gives the average voltage power density. The thermal noise, in units of charge, is expressed by Parseval's theorem,[17]

$$\sigma_{thermal}=\sqrt{C_{pd}^2\int_0^\infty |H_{pix}(\omega)|^2\overline{v_{thermal}^2}d\omega}, \tag{2}$$

where $\omega=2\pi f$, and f is frequency. In the equation, $H_{pix}(\omega)$ is the frequency-dependent transfer function formed by the pixel-preamplifier network and is given by

$$|H_{pix}(\omega)|=\frac{1}{\sqrt{\left(\frac{C_{pd}+C_{in}^*}{C_{in}^*}\right)^2+(\omega R_{on}C_{pd})^2}}. \tag{3}$$

In this equation, C_{in}^* is the effective capacitance at the preamplifier input node presented to the thermal noise voltage and is expressed as $C_{in}^*=C_{data}+AC_{fb}$. Assuming an ideal op-amp for which the open-loop voltage gain A is infinitely large and independent of frequency, Eq. (3) can be simplified with the approximation $(C_{pd}+C_{in}^*)/C_{in}^*\approx 1$. Using this approximation, and substituting Eqs. (1) and (3) into Eq. (2), the expression becomes

$$\sigma_{thermal}\approx\sqrt{kTC_{pd}}. \quad (\text{if } C_{in}^*\gg C_{pd}). \tag{4a}$$

Each time the TFT is turned off, the amount of noise determined by Eq. (4a) will be integrated in the capacitance of the photodiode. When the TFT is turned on again for the next data frame, the preamplifier samples the thermal noise, $\sigma_{thermal}$, from the TFT as well as the thermal noise, $\sigma_{thermal}$, integrated on the photodiode from the previous frame. Since the two noise contributions are equal and uncorrelated, the

total TFT thermal noise sampled by the preamplifier is increased by a factor of $\sqrt{2}$. Therefore, under typical data acquisition conditions where switching between the TFT-on and TFT-off states is continuous, the total TFT thermal noise (in units of electrons) is given by

$$\sigma_{\text{TFT-thermal}} \approx \frac{1}{q}\sqrt{2kTC_{\text{pd}}} \quad (e^-), \tag{4b}$$

where q is the electron charge. In order to account for the limited sampling time of the preamplifier, τ_{int}, Eq. (4b) takes the form[3,18]

$$\sigma_{\text{TFT-thermal}} \approx \frac{1}{q}\sqrt{2kTC_{\text{pd}}(1-e^{-2\tau_{\text{int}}/\tau_{\text{pix}}})} \quad (e^-). \tag{4c}$$

Under typical operating conditions where τ_{int} is set to a value of at least 5 pixel time constants ($5\tau_{\text{pix}}$), Eq. (4c) asymptotically approaches the form given in Eq. (4b).

b. Shot and 1/f noise associated with leakage currents ($\sigma_{pd\text{-}on}, \sigma_{pd\text{-}off}, \sigma_{TFT\text{-}off}$): When the TFT is in the off state, leakage currents in the reverse biased photodiode and in the TFT induce shot noise contributions which are integrated in the photodiode. For each of the photodiode and TFT, the corresponding current noise density is expressed by the Schottky formula, $i_{\text{shot}} = 2qI$ (A^2/Hz),[17] where I is the leakage current in the photodiode, I_{pd}, or in the TFT, I_{TFT}. Each shot noise contribution (in units of e^-) is given by

$$\sigma_{\text{shout}} = \sqrt{\frac{I\tau}{q}} \quad (e^-), \tag{5}$$

where τ corresponds to the TFT-off time, $\tau_{\text{TFT-off}}$. As in the case of TFT thermal noise, the expression for shot noise can be generalized to account for the limited sampling time of the preamplifier.

When the TFT is conducting, the photodiode generates a leakage charge proportional to the TFT-on time, $\tau_{\text{TFT-on}}$. In this case, Eq. (5) again applies, although the magnitude of the photodiode shot noise is considerably reduced since $\tau_{\text{TFT-on}}$ is typically orders of magnitude smaller than $\tau_{\text{TFT-off}}$.

Flicker ($1/f$) noise is mainly associated with the trapping and releasing of charge in the *a*-Si:H material in the photodiode and in the TFT. The magnitude of these effects is strongly influenced by the manufacturing process (i.e., the design and quality of the devices). The spectral density of $1/f$ noise is (approximately) inversely proportional to the sampling frequency, f_s, which, in turn, is equal to the inverse of the frame time, τ_{frame}. The sum of shot and $1/f$ noise can be expressed by[17]

$$\sigma = \sigma_{\text{shot}}\sqrt{1+\frac{f_L}{f_s^n}} \quad (e^-), \tag{6}$$

where σ_{shot} is given by Eq. (5). The empirical parameter f_L, known as the corner frequency, is the frequency at which the shot and $1/f$ noise components are equal. The parameter n, known as the spectral slope, determines the slope of the spectral density of the $1/f$ noise. Equation (6) is used to determine the combined magnitude of the shot and $1/f$ noise components for both the photodiode ($\sigma_{\text{pd-off}}$ and $\sigma_{\text{pd-on}}$) and for the TFT($\sigma_{\text{TFT-off}}$). Finally, in the present analysis both the shot and flicker noise components of the TFT when the TFT is conducting ($\sigma_{\text{TFT-on}}$) are assumed to be negligible.

c. Shot and 1/f noise associated with TFT transient current (σ_{tran}): In the TFT-off state, in addition to the TFT leakage current previously described, a transient current from the TFT persists after the TFT is switched off.[16] This current, which originates from the release of trapped charge from previous TFT-switching action, contributes a signal of opposite polarity compared to that of the photodiode. A noise component, σ_{tran}, associated with this transient charge can be calculated using Eq. (6). In this case, the corresponding current required for Eq. (5) decreases in an exponential-like manner due to the fact that the current depends upon the mechanism of charge release from the trapping states in the *a*-Si:H material. In model calculations, the product $I\tau$ in Eq. (5) was replaced by an empirical determination of the transient charge, Q_{tran}.[16]

Since all pixel noise components are uncorrelated to each other, they add in quadrature leading to the following expression:

$$\sigma_{\text{pix}} = \sqrt{\sigma^2_{\text{TFT-thermal}} + \sigma^2_{\text{pd-on}} + \sigma^2_{\text{pd-off}} + \sigma^2_{\text{TFT-off}} + \sigma^2_{\text{tran}}}. \tag{7}$$

A summary of the various noise components appearing in Eq. (7) is contained in Table II.

2. Preamplifier noise (σ_{amp})

Figure 3(c) is an equivalent circuit for preamplifier noise for the design of the preamplifier used in the measurements. The equivalent input noise source of the preamplifier is mostly determined by its first stage differential input transistor pair. For an identical pair of metal–oxide–semiconductor field effect transistors (MOSFETs) the voltage noise density is $\sqrt{4kT(2)(\frac{2}{3})(1/g_m)}(\text{V}/\sqrt{\text{Hz}})$,[17,19] where g_m is the transconductance of the MOSFETs, the factor $(\frac{2}{3})$ is a parameter value for MOSFET device, and the factor 2 is introduced to account for the two transistors. The input leakage current noise density, i_{amp} (appearing in Fig. 2), is usually negligible for MOS transistors and is therefore ignored. The input capacitance consists of the data line capacitance, C_{data}, and the internal input capacitance of the preamplifier, C_{amp}. The noise charge at the preamplifier input can be calculated as follows:[19]

$$\sigma_{\text{amp}} = \frac{1}{q}\sqrt{2}(C_{\text{data}}+C_{\text{amp}})\sqrt{4kT\frac{2}{3}\frac{2}{g_m}\frac{\pi}{2}f_0} \quad (e^-), \tag{8}$$

where f_0 and $(\pi/2)f_0$ are the signal and noise bandwidths of the preamplifier, respectively. The factor $\sqrt{2}$ accounts for the effect of double sampling on the noise. The bandwidth f_0 is a function of a number of parameters including the input capacitance load, the feedback capacitor, the biasing condition of the first stage transistor pair, as well as the preamplifier time constant $R_{\text{samp}}C_{\text{samp}}$ [where R_{samp} and C_{samp} are parts of the preamplifier circuit as shown in Fig. 1(b)]. For the preamplifier used in the study, C_{samp} is fixed and R_{samp} can be set (programmed) to one of four different values,

thereby allowing variation of the bandwidth. While decreasing bandwidth reduces preamplifier noise, it also results in slower readout speeds. Therefore, striking a compromise between preamplifier noise and readout speed is facilitated by the ability to vary the bandwidth through adjustment of R_{samp}.

3. Data-line thermal noise (σ_{data})

Figure 3(d) shows a simplified circuit for the data line thermal noise. The capacitance and resistance of the data line, which in reality are continuously distributed along the full length of the data line trace, are simplified and represented by two bulk capacitors, each with capacitance $C_{\text{data}}/2$, which are assumed to be distributed on either side of a bulk resistor, R_{data}. The data line noise is generated by thermal voltage fluctuations along the data line resistance, R_{data}, and the equivalent voltage noise density is given by a formula of the same form as Eq. (1). In the figure, for the noise voltage coming from the data line, the preamplifier input node serves as a virtual ground and bypasses the two capacitors ($C_{\text{data}}/2$ and C_{amp}) at the preamplifier input. Therefore, these two capacitors do not store the thermal noise charge. Rather the noise charge is stored only in the capacitor at the left side of R_{data}. Furthermore, since the time constant for the data line ($R_{\text{data}}C_{\text{data}}$, typically $\ll 1\ \mu$s) is small compared to that of the preamplifier, it corresponds to a higher bandwidth. As noise is limited by the RC circuit (which acts as a low pass filter) with the lowest bandwidth, it is reasonable to assume that data line thermal noise will be limited by the preamplifier bandwidth, f_0. [This assumption is different from the case of TFT thermal noise where the validity of Eq. (4a) depends upon the assumption that the noise is bandwidth-limited by the pixel time constant, not by the preamplifier bandwidth.] Under these conditions, the data line thermal noise charge at the preamplifier input is given by

$$\sigma_{\text{data}}=\frac{1}{q}\sqrt{2}\,\frac{C_{\text{data}}}{2}\,\sqrt{4kTR_{\text{data}}\frac{\pi}{2}f_0}\quad (e^-), \tag{9}$$

where the factor $\sqrt{2}$ is introduced to account for the effect of double sampling.

4. Externally coupled noise (σ_{ext})

The noise from external voltage supplies as well as from environmental electromagnetic interference (EMI), can all couple to each preamplifier, primarily through its data line. In Fig. 2, all of these noise components are collectively referred to as externally coupled noise and symbolically represented by an equivalent noise voltage density, v_{ext}. In practice, reducing these noise contributions to a level where the system is limited by other more intrinsic noise (e.g., thermal noise) is a nontrivial task. The level of the external noise largely depends on the following factors: the quality of the voltage supplies, the effectiveness of the shielding for the electromagnetically sensitive parts (especially the array) of the system, and the EMI of the environment. Furthermore, due to the structural uniformity among data lines and the preamplifiers, the external noise tends to couple to each data channel equally resulting in a correlated noise component.

5. Digitization noise (σ_{dig})

The process of analog to digital conversion involves a quantization noise. Theoretically, the magnitude of this noise depends only on the resolution of the ADC and the magnitude of the analog signal. For an otherwise noise-free ADC circuit, the quantization noise is given by the expression[20]

$$\sigma_{\text{dig}}=\frac{1}{q}\,\frac{Q_{\text{signal}}}{\sqrt{12}\times 2^{\text{bits}}}\quad (e^-), \tag{10}$$

where Q_{signal} is the maximum signal charge that can be digitized and *bits* is the effective resolution of the ADC in units of bits.

6. Total additive noise (σ_{add})

The total additive noise of an imaging system, σ_{add}, is the sum in quadrature of the uncorrelated individual noise components (pixel noise, σ_{pix}, preamplifier noise, σ_{amp}, data line thermal noise, σ_{data}, externally coupled noise, σ_{ext}, and digitization noise, σ_{dig})

$$\sigma_{\text{add}}=\sqrt{\sigma_{\text{pix}}^2+\sigma_{\text{amp}}^2+\sigma_{\text{data}}^2+\sigma_{\text{ext}}^2+\sigma_{\text{dig}}^2}=\sqrt{\sigma_{\text{pix}}^2+\sigma_{\text{base}}^2}, \tag{11}$$

where σ_{pix} is given by Eq. (7). In Eq. (11), σ_{base} denotes the base noise of the system, excluding pixel noise components, and is given by

$$\sigma_{\text{base}}=\sqrt{\sigma_{\text{amp}}^2+\sigma_{\text{data}}^2+\sigma_{\text{ext}}^2+\sigma_{\text{dig}}^2}. \tag{12}$$

C. Noise measurement methodology

In order to investigate the validity of the additive noise model described in this paper, measurements of the additive noise were performed to allow direct, detailed comparisons between empirically determined quantities and model predictions. These measurements consisted of determination of both the total additive noise, σ_{add}, as well as of a number of its components and involved the use of the active matrix flat-panel imager described previously. Specifically, the quantities σ_{pix}, σ_{tran}, σ_{thermal}, σ_{amp}, and σ_{data}, or combinations of these quantities, were determined and compared as they were both empirically accessible and inherently interesting in the context of model validation. Determination of these noise components necessitated measurements with the array connected to the electronic acquisition system as well as measurements in the absence of the array. In addition, obtaining these components necessitated the elimination of other noise components (σ_{base}, σ_{dig}, and σ_{ext}), which are otherwise not of interest in the context of model prediction comparisons. This was accomplished through empirical determination of σ_{base}, calculation of σ_{dig}, and direct elimination of σ_{ext} by means of an analysis technique.

In order to further test the validity of the model, noise measurements were performed as a function of the independent variables frame time, τ_{frame}, and preamplifier integra-

tion time, τ_{int}. In addition, for measurements performed in the absence of the array (σ_{amp} and σ_{data}), preamplifier input capacitance (C_{data}) and resistance (R_{data}) were also treated as independent variables by replacing the array with discrete resistors and capacitors. For array measurements as a function of τ_{frame}, this parameter was varied from ~1.8 ms up to 10 s, with τ_{int} fixed at 150 μs. For measurements as a function of τ_{int}, this parameter was varied from 5 to 150 μs with τ_{frame} fixed at ~1.8 ms. Finally, for measurements as a function of C_{data}, this parameter was varied from 0 to 136 pF with τ_{frame} and τ_{int} fixed at ~1.8 ms and 150 μs, respectively. In this case, values for R_{data} of 0, 5, 10, and 20 kΩ were used. For all noise measurements with the array connected to the electronic acquisition system, the photodiode bias voltage, V_{bias}, was fixed at -6 V.

For all array measurements, a data acquisition sequence consisting of a number of consecutive frames (''readout cycles'') was performed. While initial frames (10 000, for most measurements) were discarded in order to establish equilibrium between charge trapping and charge release in the *a*-Si:H photodiodes,[2] the remaining frames (typically 100) were saved and used for data analysis. Data analysis consisted of calculating the standard deviation in the mean signal for each pixel over the samples (i.e., frames) obtained. In the case of noise measurements performed in the absence the array, the system was operated in a manner very similar to when the array was present and noise data were obtained by directly probing the output signal of the preamplifier with a digital oscilloscope.

1. Measurement of total additive noise (σ_{add})

Measurements of the total additive noise were conducted using the sampling method shown in Fig. 1(c) and previously discussed. Data were acquired for all pixels in a small, contiguous region of the array (7×2 pixels or 16×1 pixels [data$\times$gate]). Signals from nonaddressed pixels were prevented from contributing to the measurements by maintaining a negative voltage (V_{off}) to the corresponding gate lines.

2. Elimination of externally coupled noise (σ_{ext})

The externally coupled noise associated with voltage supplies within the acquisition electronics or from outside electromagnetic sources produces a correlated noise component at the preamplifier input, also referred to as line noise. In an image, this noise manifests itself as striations along the gate line direction. Since pixels on a given gate line incur the same voltage fluctuations during readout, it is therefore possible to remove their common systematic signal variations. This correlated noise component was eliminated by using a pair of neighboring pixels lying on the same gate line. For each data sample, subtraction of the signals for the pixel pair yields a response free of correlated noise. Analysis is then performed on this difference with the resulting standard deviations divided by $\sqrt{2}$ to account for additional uncorrelated noise introduced by the subtraction. This method has proven to be very effective in reducing all external noise components due to their highly correlated nature. In the present study, because external noise can vary from one measurement to the next, this ''correlated noise subtraction method'' was applied so as to eliminate its contribution.

3. Measurement of system base noise (σ_{base}) and pixel noise (σ_{pix})

The noise associated with the acquisition system, σ_{base}, was measured using a timing procedure similar to that used for the total additive noise measurement. However, in this case all 512 gate lines of the array were kept at a negative voltage, V_{off}, so that signal sampling by the preamplifier was performed in the absence of pixel signal. Moreover, since under these conditions all pixels along a data line are isolated from the line by the large TFT-off resistance, R_{off}, their noise contribution is negligible. In addition, all the gate lines were inspected to ensure that there were no defective or floating gate lines, which would otherwise contribute extra noise due to TFT leakage. Finally, pixel noise was determined through subtraction in quadrature of the results of the measurements of total additive noise and base noise.

4. Measurement of preamplifier noise (σ_{amp}) and data line thermal noise (σ_{data})

When the array is attached to the electronic acquisition system, it is not possible to directly measure the preamplifier and data line thermal noise components individually. However, their combined magnitude, $\sqrt{\sigma_{amp}^2+\sigma_{data}^2}$, can be inferred from the measurement of the system base noise, σ_{base}, when the other components of σ_{base} (i.e., digitization noise and externally coupled noise) are eliminated. While external noise was experimentally removed by means of the correlated noise subtraction method described above, digitization noise was removed via calculation of σ_{dig} using Eq. (10).

Furthermore, in order to determine the magnitudes of σ_{amp} and σ_{data} separately so as to test model predictions for these quantities, the circuit shown in Fig. 3(d) was assembled using discrete component capacitors and resistors (in the absence of the array) at the input of the preamplifiers. For a given value of R_{data}, the noise representing $\sqrt{\sigma_{amp}^2+\sigma_{data}^2}$ was measured as a function of capacitance, C_{data}. The measurement at a value for R_{data} of 0 Ω corresponds to the case of the data line thermal noise contribution approaching zero, thereby providing a direct measure of preamplifier noise. This knowledge of σ_{amp}, in turn, allowed the magnitude of σ_{data} to be extracted from the aforementioned array measurement of $\sqrt{\sigma_{amp}^2+\sigma_{data}^2}$. To further test the model, measurements of $\sqrt{\sigma_{amp}^2+\sigma_{data}^2}$ were also performed (in the absence of the array) as a function of preamplifier bandwidth, with f_0 ranging from 135 to 230 kHz and R_{data} and C_{data} fixed at 5 kΩ and 66 pF, respectively. In these measurements, the preamplifier gain was reduced (corresponding to an increase in preamplifier charge capacity from ~4 pC to ~23 pC) in order to allow a larger range of bandwidth values. For all measurements of $\sqrt{\sigma_{amp}^2+\sigma_{data}^2}$, the bandwidth was empirically determined.

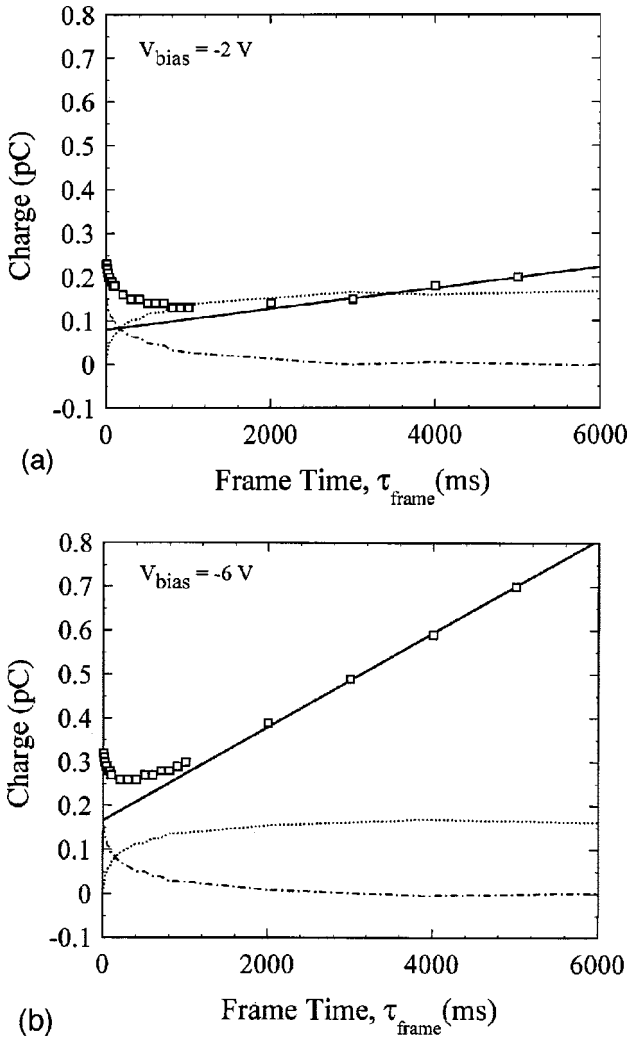

FIG. 4. Measurements of pixel dark signal (squares) plotted as a function of frame time, τ_{frame}. Data are shown for a photodiode bias voltage, V_{bias} of (a) -2 V, and (b) -6 V. Due to the contribution of an unknown amount of charge from TFT switching and the preamplifier circuit, these data contain an arbitrary offset and thus represent relative, not absolute, magnitudes. For each data set, the solid line represents a linear fit to the pixel dark signal measurements at long frame times. The dotted–dashed line represents charge remaining in the TFT which is yet to be released as TFT transient charge. The dotted line represents the cumulative TFT transient charge. See main text for details.

5. Measurement of TFT transient noise (σ_{tran}) and TFT thermal noise ($\sigma_{thermal}$)

In the measurements, the TFT transient noise could not be determined separately from the TFT thermal noise since both components derived from TFT switching. However, the quantity $\sqrt{\sigma_{\text{tran}}^2+\sigma_{\text{thermal}}^2}$ was empirically determined and compared with model predictions. The determination of this quantity involved the readout of only a single row of pixels per frame. Two types of measurements were performed at the minimum frame time ($\sim$1.8 ms) in order to render the photodiode and TFT shot noise contributions, $\sigma_{\text{pd-off}}$ and $\sigma_{\text{TFT-off}}$, negligible. The first was a measurement of the total additive noise of the system, σ_{add}, performed as described above. The second used the same measurement technique

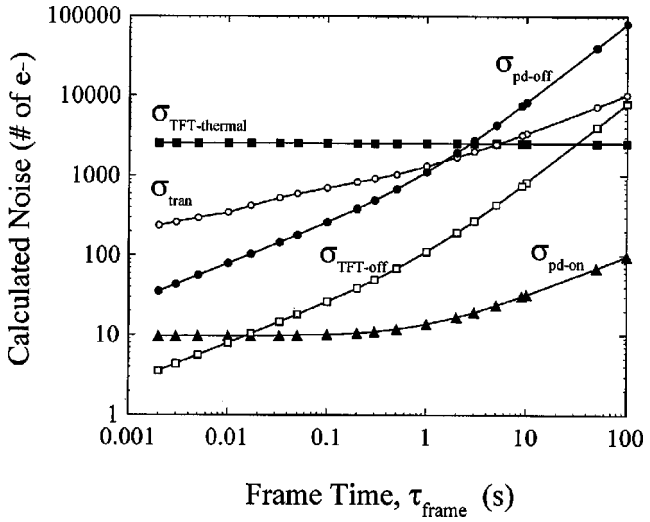

FIG. 5. Noise model calculations of the various components of pixel noise plotted as a function of frame time. As for all calculations appearing in the following figures, these predictions correspond to the array design summarized in Table I and the values represent RMS noise, referred to the input of the preamplifier. The calculations for $\sigma_{\text{TFT-thermal}}$, σ_{tran}, $\sigma_{\text{pd-off}}$, $\sigma_{\text{TFT-off}}$, and $\sigma_{\text{pd-on}}$ are indicated by solid squares, open circles, solid circles, open squares, and solid triangles, respectively. The lines joining the points are included for clarity of presentation.

employed for total additive noise except for the fact that the TFTs of the selected gate line were continually maintained in the on state. The second measurement was subtracted in quadrature from the first. The square root of these subtracted values is equal to $\sqrt{\sigma_{\text{tran}}^2+\sigma_{\text{thermal}}^2}$ since the second measurement excludes the TFT transient noise contribution as well as the contribution of TFT thermal noise from the previous frame.

D. Determination of noise model parameters

In the model, five components of pixel noise are specified, as indicated in Eq. (7). Calculations of $\sigma_{\text{TFT-thermal}}$ were performed using Eq. (4b) while calculations of $\sigma_{\text{TFT-off}}$, $\sigma_{\text{pd-off}}$, $\sigma_{\text{pd-on}}$, and σ_{tran} were performed using Eq. (6). For each component, the parameters used in the model calculations were either known from the array design (as summarized in Table I), empirically determined using the imaging system, or assumed. For the $\sigma_{\text{TFT-thermal}}$ calculations, the photodiode capacitance, C_{pd}, was determined to be $\sim$20 pF (using the measurement technique reported in Ref. 2 and a temperature, T, of 295 K was assumed). In Eq. (6), the value of the corner frequency, f_L, depends upon the manufacturing process and may vary from pixel to pixel on the same array. For purposes of the present study, a central value of $f_L=1$ Hz is assumed.[18] In addition, the parameter n, which typically varies from 0.8 to 1.3 for various devices,[21] was set to a value of 1 for the TFTs and the photodiodes.

For the calculation of each of $\sigma_{\text{pd-off}}$, $\sigma_{\text{pd-on}}$, and σ_{tran}, the value used for the corresponding shot noise contribution, σ_{shot}, was derived from Eq. (5) using the product of an empirically determined leakage current, I, and the appropriate time interval, τ, or using a direct measurement of the leakage

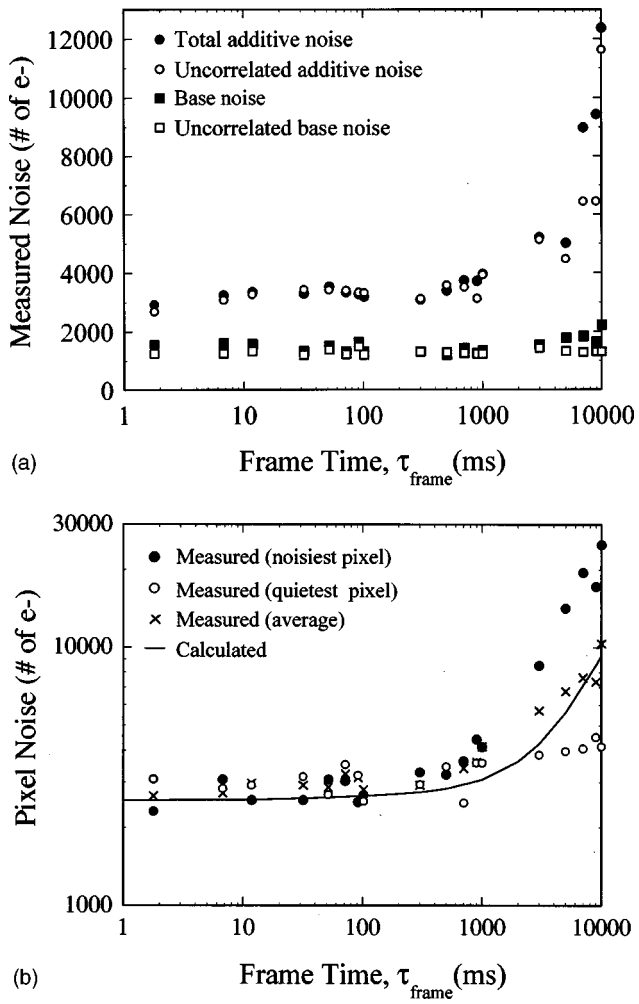

FIG. 6. Noise measurements plotted as a function of frame time. (a) Total additive noise before and after the application of the correlated noise subtraction method (solid and open circles, respectively); base noise before and after correlated noise subtraction (solid and open squares, respectively). (b) Pixel noise, σ_{pix}, derived from the correlated-noise-subtracted total additive noise and base noise data shown in (a). Three sets of pixel noise results, corresponding to the noisiest pixel (solid circles), the quietest pixel (open circles), and the average behavior of all sampled pixels (crosses), are shown. The line corresponds to noise model calculations.

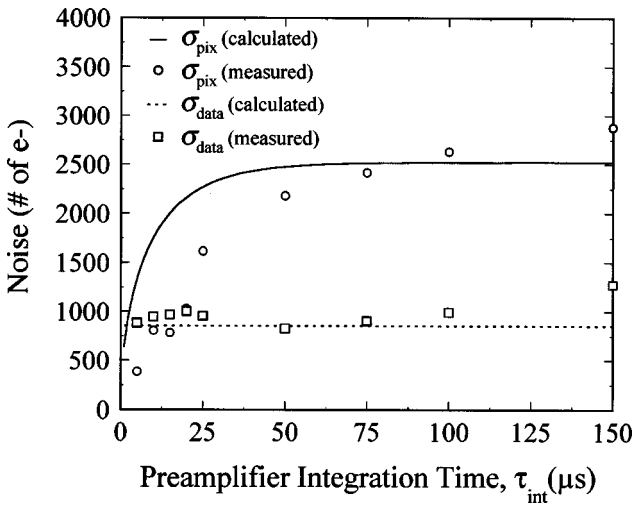

FIG. 7. Measurements of pixel noise, σ_{pix}, (circles) and data line thermal noise, σ_{data}, (squares) plotted as a function of preamplifier integration time. The solid and dashed lines correspond to noise model calculations of σ_{pix} and σ_{data}, respectively.

charge, $I\tau$. (In the case of $\sigma_{TFT\text{-}off}$, a leakage current of 1 fA was assumed.[18]) For the calculations associated with the TFT-on state ($\sigma_{pd\text{-}on}$) and the TFT-off state ($\sigma_{pd\text{-}off}$ and $\sigma_{TFT\text{-}off}$), τ was given by preamplifier integration time, τ_{int}, and frame time, τ_{frame}, respectively.

Figures 4(a) and 4(b) contain measurements of the relative magnitude of the total pixel dark signal (squares), plotted as a function of τ_{frame} for photodiode bias voltages, V_{bias}, of -2 V and -6 V, respectively. The pixel dark signal includes contributions from photodiode and TFT leakage currents, the TFT transient current, and charge originating from TFT switching and the preamplification circuit.[2] The minimum observed in the data at low frame times is due to the contribution of the TFT transient current, which is opposite in polarity to the photodiode current and decreases with increasing τ_{frame}. At frame times beyond this minimum, the TFT transient current becomes negligible and the dark signal increases in a linear manner. The slope of this linear region (represented by a solid line in each figure) corresponds to a leakage current of ~25 fA and ~110 fA for the -2 V and -6 V data, respectively. These values were assumed to represent a reasonable estimate of the photodiode leakage current in the TFT-off state, given the comparatively smaller leakage current assumed for the TFT. (It was also assumed that the same photodiode leakage currents applied for the calculations of $\sigma_{pd\text{-}on}$.)

In the case of the σ_{tran} calculations, the transient charge, Q_{tran}, required for the shot noise parameter calculations, was determined as follows. For a given value of frame time, the difference between the measured pixel dark signal and the solid line in each of Figs. 4(a) and 4(b) corresponds to the absolute magnitude of the amount of trapped charge in the TFT yet to be released via the TFT transient current.[16] This magnitude, represented by the dotted–dashed lines in the figures, is a maximum at τ_{frame} equals zero, and asymptotically approaches zero at higher frame times. The magnitude of this maximum is ~165 fC and represents the total amount of charge deposited in the photodiode by the TFT transient current at long frame times, $Q_{tran\text{-}max}$. In each figure, the dotted curve, obtained by subtracting the dotted-dashed curve from $Q_{tran\text{-}max}$, corresponds to the amount of TFT transient charge deposited in the photodiode (i.e., Q_{tran}) as a function of τ_{frame}. A careful comparison of the dotted lines in the two figures indicates that the results are independent of V_{bias}, as would be expected.

III. RESULTS

A. Pixel noise (σ_{pix})

1. Dependence on frame time (τ_{frame})

Model predictions for each of the individual components of pixel noise, plotted as a function of frame time, are shown in Fig. 5. The figure shows that TFT thermal noise, which is

independent of τ_{frame}, is the dominant component for short frame times (i.e., $\lesssim$1 s). At higher frame times, shot and flicker noise, which are associated with the photodiode and TFT transient leakage currents, increase with increasing frame time and eventually become the dominant components.

Figure 6(a) shows measurements of the total additive noise of the system, σ_{odd}, plotted as a function of frame time. Results are shown before (solid circles) and after (open circles) the application of the previously described correlated noise substraction method used to eliminate σ_{ext}. The effect of removing σ_{ext} is relatively small for most of the data, indicative of modest correlated noise contributions. (The comparatively larger correlated noise contributions observed for a few of the measurements were possibly due to intermittent environment electromagnetic interference.) Measurements of system base noise, σ_{base} before (solid squares) and after (open squares) correlated noise subtraction are also shown in the figure. These results indicate that, for the present imaging system, σ_{base} is independent of frame time and that it represents only a relatively small contribution to the total additive noise.

Three sets of pixel noise measurements, σ_{pix}, are plotted in Fig. 6(b). Two of these sets correspond to individual pixels exhibiting the highest (solid circles) and lowest (open circles) levels of noise observed, while the third set (crosses) corresponds to the average from all (7×2) sampled pixels. The large measured variations between individual pixels at long frame times could be due to significant pixel-to-pixel variations in the corner frequency, f_L. The figure also shows model calculations for σ_{pix} (line) which correspond to the sum of all of the individual noise components shown in Fig. 5. In general, there is reasonable agreement between the measurements and theory.

2. Dependence on preamplifier integration time (τ_{int})

In Fig. 7, model calculations (solid line) and measurements (circles) of pixel noise are shown as a function of preamplifier integration time, τ_{int}. Under the conditions of the measurements and calculations (i.e., $\tau_{\text{frame}}=1.8$ ms) the pixel noise is completely dominated by the TFT thermal noise component. While the theoretical predictions are in reasonable agreement with the measurements at values of τ_{int} greater than the pixel time constant, $\tau_{\text{pix}}(\sim30\,\mu\text{s})$, at shorter values of τ_{int} the data exhibit a considerably steeper decrease than the calculations. It is interesting to point out that replacing the factor of 2 in the exponent of Eq. (4c) with unity considerably improves the agreement at shorter values of τ_{int} while leaving the results at longer values of τ_{int} unaffected. However, in any case, imaging systems are normally operated at preamplifier integration times at least five times larger than the pixel time constant in order to insure maximum collection of the pixel signal.

The diminution of pixel noise, σ_{pix}, with decreasing τ_{int} originates from the fact that as the preamplifier integration time becomes short compared to τ_{pix}, the collection of pixel signal by the preamplifier becomes increasingly incomplete thereby leading to a truncated measurement of pixel signal and noise. In principle, the same effect could occur with data line thermal noise given the parallels between data line thermal noise and TFT thermal noise. However, since the time constant of a data line is typically quite small (e.g., $R_{\text{data}}C_{\text{data}}\approx0.8\,\mu$s for the present array), it is unlikely that an

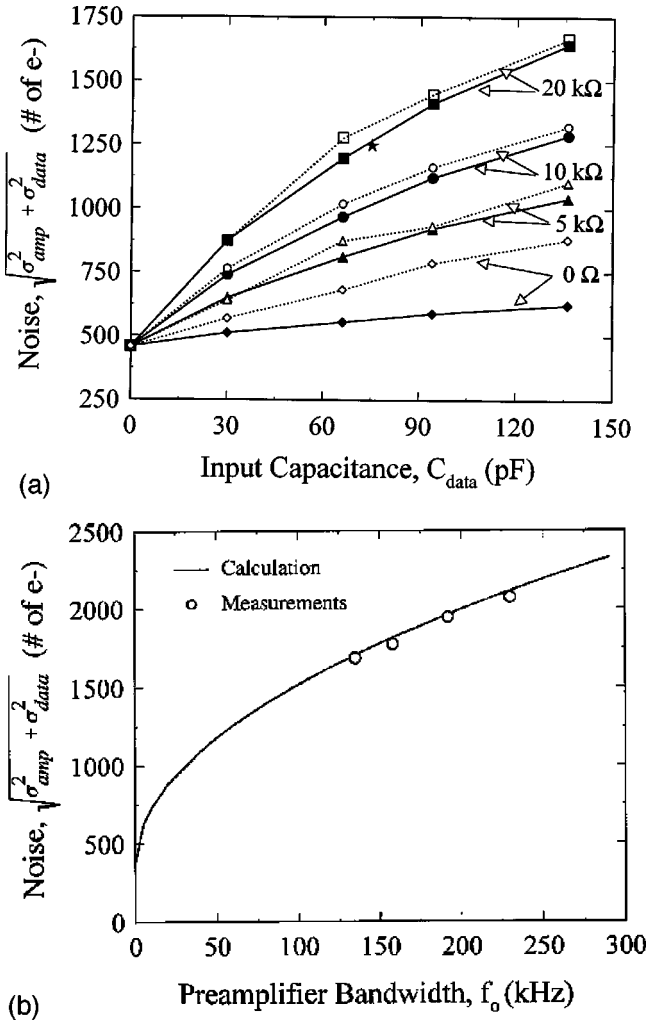

FIG. 8. Measurements and calculations of the combined preamplifier and the data line thermal noise components, $\sqrt{\sigma^2_{\text{amp}}+\sigma^2_{\text{data}}}$. (a) Measurements obtained in the absence of the array for input resistance, R_{data}, values of 0, 5, 10, and 20 kΩ indicated by open diamonds, triangles, circles, and squares, respectively. These results are plotted as a function of input capacitance to the preamplifier, C_{data}. Noise model calculations corresponding to the conditions of the measurements are shown by the solid symbols. These calculations utilize the measured value of the bandwidth and also include an offset of $365\,e^-$ which was added in order to account for the effect of extraneous noise contributions which were present in the corresponding (nonarray) measurements. The lines in the figure joining the points are included for clarity of presentation. In addition, the result of a single measurement of $\sqrt{\sigma^2_{\text{amp}}+\sigma^2_{\text{data}}}$, obtained with the array connected to the acquisition electronics, is shown by a star. Note that in this figure, the *y*-axis starts from $250\,e^-$. (b) Measurements obtained in the absence of the array (open circles) plotted as a function of the preamplifier bandwidth, f_0. These results were obtained using a fixed value of 5 kΩ for R_{data} and 66 pF for C_{data}. Noise model calculations corresponding to the conditions of the measurements are shown by a solid line. These calculations include the same offset of $365\,e^-$ as used in (a).

imaging system would be operated under conditions where the selected value of τ_{int} is sufficiently small that any effect would be observed. For example, in Fig. 7 measurements of σ_{data} (squares) as a function of τ_{int} remain essentially unchanged. Furthermore, the magnitude of these measurements is consistent with the value for σ_{data} predicted by the model (dashed horizontal line).

B. TFT transient noise (σ_{tran}) and TFT thermal noise ($\sigma_{thermal}$)

Model predictions for the pixel noise components associated with the TFT switching action, σ_{tran} and $\sigma_{thermal}$, are 240 e^- and 1790 e^-, respectively, at a frame time of 1.8 ms. Their combined magnitude, $\sqrt{\sigma_{tran}^2+\sigma_{thermal}^2}$, of ~1810 e^- is in reasonable agreement with a measured value of ~2140 e^-, given an estimated measurement precision of approximately ±300 e^-. In addition, a measurement of pixel noise, σ_{pix}, at the same frame time, yielded a value of ~2600 e^-. At this value of τ_{frame}, TFT thermal noise is by far the dominant component of σ_{pix} and the model predicts a value of ~2530 $e^-(\sqrt{2}\sigma_{thermal})$, which is in good agreement with the σ_{pix} measurement. This detailed examination of the contribution of $\sigma_{thermal}$ to additive noise, strongly supports the manner in which the phenomenon of TFT thermal noise has been represented in the model.

C. Preamplifier noise (σ_{amp}) and data line thermal noise (σ_{data})

Figure 8(a) shows measurements of preamplifier and data line thermal noise, $\sqrt{\sigma_{amp}^2+\sigma_{data}^2}$ (open symbols) obtained in the absence of the array through the use of discrete components connected to the input of the preamplifier. The noise was measured as a function of input capacitance, C_{data}, for a variety of input resistance values, R_{data}, ranging from 0 to 20 kΩ. The corresponding noise model calculations are also shown (solid symbols). In these calculations, the magnitude of the preamplifier bandwidth varied (from ~9 to ~69 kHz) with input capacitance, C_{data}, and was determined through direct measurements at each value of C_{data}. Generally, the results indicate that $\sqrt{\sigma_{amp}^2+\sigma_{data}^2}$ increases both with input capacitance and input resistance. The agreement between model calculations and measurements is fairly good for nonzero input resistance. At zero input resistance, which corresponds to the case of no contribution from the data line thermal noise, discrepancies between theory and measurements increase with increasing C_{data}. This disagreement may be due to additional preamplifier noise contributions that are not accounted for in the model. A measurement of $\sqrt{\sigma_{amp}^2+\sigma_{data}^2}$ with the array connected to the electronic acquisition system is also shown in the figure (indicated by a star). (In the case of the array measurement, R_{data} and C_{data} are estimated to be ~10 kΩ and ~75 pF, respectively.) The difference between the array measurement, ~1250 e^-, and the value to be expected based on interpolation of measurements involving discrete components, ~1050 e^-, is within the precision of the experimental techniques.

TABLE III. Model calculations of various additive noise components (in units of electrons) for hypothetical AMPFI imaging systems incorporating 100, 200, and 400 μm pixel-to-pixel pitch arrays. In the calculations, the array design characteristics and performance specifications were generally based on design parameters representative of current state-of-the-art arrays as well as on the 508 μm pitch array design used in the measurements. The calculations assume an array size of 40×40 cm^2, a data line capacitance based on 25 fF per pixel (Ref. 12), a data line resistance based on 0.4 kΩ per cm, and a value for g_m [see Eq. (8)] of 8 mA/V (corresponding to that of the preamplifiers used in the measurement). In addition, 16-bit resolution analog-to-digital converters, a frame time of 100 ms and a preamplifier bandwidth, f_0, of $1/\pi\tau_{pix}$ (where τ_{pix} scales with the pixel pitch) were assumed. The photodiodes were assumed to have a capacitance per unit area of 89.7 pF/mm^2 (corresponding to that of the 508 μm array) and a fill factor (Ref. 2) of 80%. The TFT size was assumed to be 12 μm×9.5 μm (Ref. 22) giving a TFT-on resistance R_{on} of ~6.6 MΩ (Ref. 2) at V_{on} equals 10 V. In the calculation of σ_{dig} using Eq. (10), Q_{signal} was set to the pixel charge capacity which was obtained assuming a photodiode bias voltage of −6 V (Ref. 2). Finally, the externally coupled noise component, σ_{ext}, was assumed to be negligible.

Pixel pitch (μm)	100	200	400
Pixel noise, σ_{pix}	490	960	1910
Data line thermal noise, σ_{data}	2310	580	140
Preamplifier noise, σ_{amp}	560	160	50
ADC Digitization noise, σ_{dig}	120	480	1900
Total electronic noise, σ_{add}	2430	1240	2730

Figure 8(b) shows measurements of $\sqrt{\sigma_{amp}^2+\sigma_{data}^2}$ in the absence of the array as a function of the preamplifier bandwidth. The measurements were conducted for a fixed input capacitance and input resistance ($R_{data}=5$ kΩ, $C_{data}=66$ pF) at four different preamplifier bandwidths. The solid line shown in the figure represents model predictions which accurately reproduce the trend observed in the measurements.

IV. SUMMARY AND DISCUSSION

A detailed theoretical and empirical investigation of additive noise for indirect detection, active matrix flat-panel imagers has been performed. Such imagers comprise a pixelated array, incorporating photodiodes and thin-film transistors, and an associated electronic acquisition system. A theoretical model of additive noise, defined as the noise of an imaging system in the absence of radiation, has been developed. This model is based upon an equivalent-noise-circuit representation of an AMFPI. The model contains a number of uncorrelated noise components which have been designated as pixel noise, data line thermal noise, externally coupled noise, preamplifier noise and digitization noise. Pixel noise is further divided into the following components: TFT thermal noise, shot and $1/f$ noise associated with the TFT and photodiode leakage currents, and TFT transient noise.

An examination of the validity of the model was performed through detailed comparisons of model calculations with empirical results. These empirical results were obtained through measurements involving a 26×26 cm^2, 508 μm pixel-to-pixel pitch active matrix array connected to an electronic acquisition system as well as through measurements

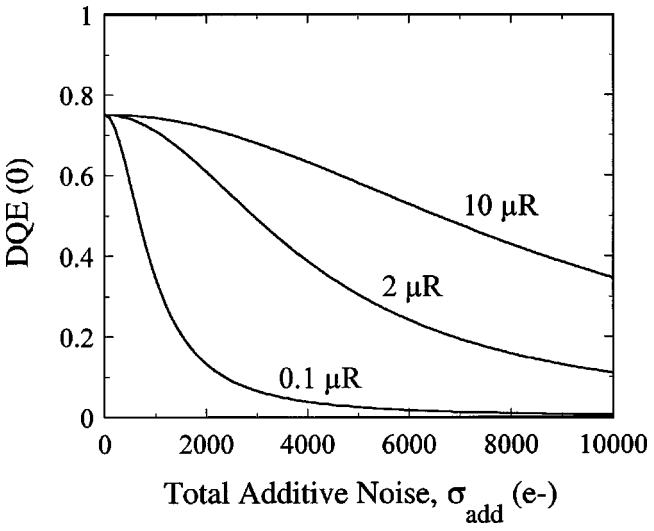

FIG. 9. Zero-frequency DQE calculations for a hypothetical, indirect detection, active matrix flat-panel imager incorporating a 200 μm pitch array with an 80% fill factor. In addition, a 500 μm thick CsI(Tl) converter is assumed. The calculations were performed using a model based on cascaded systems formalism (Ref. 3). The calculations are presented as a function of total additive noise at an x-ray energy of 80 kVp for three values of exposure to the detector spanning the range of the fluoroscopic application (i.e., min., max., and mean exposures) (Refs. 3 and 5). In these calculations, the effect of noise power aliasing (Ref. 23) is not included.

performed in the absence of the array (involving discrete components connected to the preamplifier input). The empirical results consisted of measurements of the total additive noise as well as measurements of pixel noise, preamplifier noise, and data line thermal noise components. Other noise components, which allowed access to the former components, were either estimated or removed. For example, digitization noise from the 16-bit ADCs used in the acquisition system was estimated to be $\sim 160e^-$. In addition, in all measurements, externally coupled noise (originating from power supplies and environmental electromagnetic interference) was reduced to the level of a few hundred electrons through careful system design and was then systematically eliminated using the analysis technique involving correlated noise subtraction previously described in Sec. II C 2.

Comparisons of model calculations and measurements of the pixel noise component as a function of frame time and preamplifier integration time generally demonstrated good agreement. The model indicates that, at frame times above $\sim$1 s, shot and $1/f$ noise components of the photodiode and TFT increase rapidly and become the dominant components of pixel noise. At shorter frame times, the model predicts that pixel noise is increasingly dominated by TFT thermal noise. Measurements made at an extremely short frame time ($\sim$1.8 ms) isolated two independent contributions of TFT thermal noise. The reasonable degree of agreement between these measurements and model predictions provide strong evidence that the relatively complex role of TFT thermal noise has been properly incorporated into the model as well as support the prediction of dominance by TFT thermal noise contributions at short frame times.

Preamplifier noise and data line thermal noise components have been modeled using equivalent circuits to represent individual array data lines by discrete capacitors and resistors. The noise model indicates that the magnitude of both of these noise components is directly proportional to the preamplifier input capacitance (corresponding to the data line capacitance of the array) and to the square root of the preamplifier bandwidth. These predicted dependencies are in reasonable agreement with noise measurements performed on individual preamplifier channels using discrete RC components (simulating the data line) at their input. The model also indicates that data line thermal noise is directly proportional to the square root of the input resistance to the preamplifier (corresponding to the resistance of the data lines)—a dependence which was confirmed by the measurements. Finally, a measurement of preamplifier and data line thermal noise, obtained with the array connected to the electronics, was in agreement with measurements obtained in the absence of the array (involving discrete resistors and capacitors simulating aspects of the array), thereby helping to validate the use of discrete components to test aspects of the model which might be otherwise inaccessible using an array.

The generally good agreement observed between model calculations and measurements lends confidence to the use of the model for exploring the additive noise properties of hypothetical imaging systems. Table III contains calculations of hypothetical imaging systems incorporating a 40 $\times 40\,\mathrm{cm}^2$ array, such as could be used for radiography or fluoroscopy. Predictions of the magnitude of various noise components, as well as of the total additive noise, are shown for array designs incorporating pixel pitches of 100, 200, and 400 μm. As seen in the table, both pixel and digitization noise increase with increasing pixel pitch due to the corresponding increase in pixel charge capacity. (In the case of the digitization noise calculation, the maximum signal to be digitized was assumed to correspond to the pixel charge capacity at a given pitch.) Under the assumptions of the calculations, data line thermal noise and preamplifier noise decrease with increasing pixel pitch due to the reduction in data line capacitance as the number of pixels along the data line decreases. The predicted total additive noise is a minimum at 200 μm pixel pitch and is significantly higher at 100 μm and 400 μm pitch. This result reflects the competing effects of the various noise contributions. In these calculations, the 100 μm pixel array design, which produces the smallest pixel signal for a given exposure among the three designs, exhibits the worst signal-to-noise performance. The 200 μm pitch array, on the other hand, exhibits lower additive noise and integrates four times more signal, thus offering considerably enhanced signal-to-noise performance compared to the 100 μm design.

The model for additive noise of flat-panel imagers presented in this paper can serve as an effective tool for identifying noise components that may limit the imaging performance of a system. Such information can be valuable in the process of optimizing performance through understanding and minimization of additive noise contributions. For example, in the case of fluoroscopy which involves very low x-ray exposures per image frame, achieving low additive

noise is crucial to insuring that the system is input-quantum-limited over as much of the exposure range as possible.[3,10] Presently, the additive noise levels of active matrix flat-panel imagers are such that DQE falls sharply with decreasing exposure.[3,10] The sensitivity of the DQE performance of AMFPIs to the level of additive noise for exposures in the fluoroscopic range is illustrated in Fig. 9. This figure clearly demonstrates the strong dependence of DQE on additive noise at low exposures. Motivated by such strong indications that reductions in additive noise can significantly improve imager performance, a variety of strategies to reduce various additive noise components (e.g., through reduction of data line capacitance, improvement in preamplifier design, and the incorporation of correlated-noise-reduction techniques) are being pursued.[5,10,24] Given the large amount of effort associated with developing and implementing such improvements, the use of a reliable additive noise model in theoretical predictions of imager performance can assist in identifying and pursuing those noise reduction strategies which offer the greatest potential performance enhancements.

ACKNOWLEDGMENTS

We wish to express our thanks to John Boudry, Tom Zimmermann, and Bob Street for valuable discussions concerning the noise model. In addition, we gratefully acknowledge the support of NIH Grants Nos. RO1-CA56135 and RO1-CA76405.

[a]Author to whom correspondence should be addressed. Phone: 734-936-4309; Fax: 734-763-1369; electronic mail: manat@umich.edu
[b]Present address: Department of Diagnostic Radiology, UT M.D. Anderson Cancer Center, Houston, Texas 77030.

[1] L. E. Antonuk, Y. El-Mohri, J. Yorkston, K.-W. Jee, J. Siewerdsen, M. Maolinbay, V. E. Scarpine, and H. Sandler, ''Initial performance evaluation of an indirect-detection, active-matrix flat-panel imager (AMFPI) prototype for megavoltage imaging,'' Int. J. Radiat. Oncol., Biol., Phys. **42**, 437–454 (1998).
[2] L. E. Antonuk, Y. El-Mohri, J. H. Siewerdsen, J. Yorkston, W. Huang, V. E. Scarpine, and R. A. Street, ''Empirical investigation of the signal performance of a high-resolution, indirect detection, active matrix flat-panel imager (AMFPI) for fluoroscopic and radiographic operation,'' Med. Phys. **24**, 51–70 (1997).
[3] J. H. Siewerdsen, L. E. Antonuk, Y. El-Mohri, J. Yorkston, W. Huang, J. M. Boudry, and I. A. Cunningham, ''Empirical and theoretical investigation of the noise performance of indirect detection, active matrix flat-panel imagers (AFMPIs) for diagnostic radiology,'' Med. Phys. **24**, 71–89 (1997).
[4] L. E. Antonuk, Y. El-Mohri, W. Huang, K.-W. Jee, M. Maolinbay, V. E. Scarpine, J. H. Siewerdsen, M. Verma, J. Yorkston, and R. A. Street, ''Development of a high resolution, active matrix, flat-panel imager with enhanced fill factor,'' Proc. SPIE **3032**, 2–13 (1997).
[5] L. E. Antonuk, K.-W. Jee, Y. El-Mohri, M. Maolinbay, S. Nassif, X. Rong, Q. Zhao, and J. H. Siewerdsen, ''Strategies to improve the signal and noise performance of active matrix, flat-panel imagers for diagnostic x-ray imaging,'' Med. Phys. **27**, 289–306 (2000).
[6] K.-W. Jee, L. E. Antonuk, Y. El-Mohri, C. Cionca, M. Maolinbay, S. Nassif, and Q. Zhao, ''A theoretical investigation of advanced design active matrix flat-panel imagers for mammography,'' Proc. SPIE **3977**, 250–256 (2000).
[7] J. H. Siewerdsen, L. E. Antonuk, Y. El-Mohri, J. Yorkston, W. Huang, and I. A. Cunningham, ''Signal, noise power spectrum, and detective quantum efficiency of indirect-detection flat-panel imagers for diagnostic radiology,'' Med. Phys. **25**, 614–628 (1998).
[8] A. Rose, ''A unified approach to the performance of photographic film, television pick-up tubes, and the human eye,'' J. Soc. Motion. Picture Eng. **47**, 273 (1946).
[9] P. Munro and D. C. Bouius, ''X-ray quantum limited portal imaging using amorphous silicon flat-panel arrays,'' Med. Phys. **25**, 689–702 (1998).
[10] L. E. Antonuk, Y. El-Mohri, K.-W. Jee, M. Maolinbay, S. C. Nassif, X. Rong, J. H. Siewerdsen, Q. Zhao, and R. Street, ''Beyond the limits of present active matrix, flat-panel imagers (AMFPIs) for diagnostic radiology,'' Proc. SPIE **3659**, 518–527 (1999).
[11] E. J. Morton, L. E. Antonuk, J. E. Berry, W. Huang, P. Mody, and J. Yorkston, ''A data acquisition system for flat-panel imaging arrays,'' IEEE Trans. Nucl. Sci. **41**, 1150–1154 (1994).
[12] L. E. Antonuk, J. Boudry, Y. El-Mohri, W. Huang, J. H. Siewerdsen, and J. Yorkston, ''Large area, flat-panel, amorphous silicon imagers,'' Proc. SPIE **2432**, 216–227 (1995).
[13] R. J. Yarema, T. Zimmermann, J. Srage, L. E. Antonuk, J. Berry, W. Huang, and M. Maolinbay, ''A programmable, low noise, multichannel preamplifier for pixelated amorphous silicon arrays,'' Nucl. Instrum. Methods Phys. Res. A **439**, 413–417 (2000).
[14] U. Shiebel, N. Conrads, N. Jung, M. Weibrecht, H. Wieczorek, T. Zaengel, M. J. Powell, I. D. French, and C. Glasse, ''Fluoroscopic x-ray imaging with amorphous silicon thin-film arrays,'' Proc. SPIE **2163**, 129–140 (1994).
[15] R. E. Colbeth, M. J. Allen, D. J. Day, D. D. Gilblom, R. Harris, I. D. Job, M. E. Klausmeier-Brown, J. Pavkovich, E. J. Shapiro, M. D. Wright, and J. M. Yu, ''Flat-panel imaging system for fluoroscopy applications,'' Proc. SPIE **3336**, 376–387 (1998).
[16] R. A. Street, R. L. Weisfield, R. B. Apte, S. E. Ready, A. Moore, M. Nguyen, W. B. Jackson, and P. Nylen, ''Amorphous silicon sensor arrays for x-ray and document imaging,'' Thin Solid Films **296**, 172–176 (1997).
[17] Y. Netzer, ''The design of low noise amplifiers,'' From selected papers on *Noise in Circuits and Systems*, edited by Madhu S. Gupta (IEEE, New York, 1988), pp. 19–32.
[18] J. M. Boudry, *Evaluation of Hydrogenated Amorphous Silicon Photodiodes and Field-Effect Transistors for Use as Elements of Two-Dimensional X-Ray Imaging Arrays* (UMI Dissertation Services, Ann Arbor, MI, 1996).
[19] A. Van Der Ziel, *Noise in Measurements* (Wiley, New York, 1976).
[20] J. G. Proakis and D. G. Manolakis, *Digital Signal Processing: Principles, Algorithms, and Applications*, 3rd ed. (Prentice–Hall, New Jersey, 1996).
[21] C. D. Motchenbacher and J. A. Connely, *Low-Noise Electronics System Design* (Wiley, New York, 1993).
[22] L. E. Antonuk, Y. El-Mohri, A. Hall, K.-W. Jee, M. Maolinbay, S. C. Nassif, X. Rong, J. H. Siewerdsen, Q. Zhao, and R. Weisfield, ''A large-area, 97 μm pitch, indirect-detection, active matrix, flat-panel imager (AMFPI),'' Proc. SPIE **3336**, 2–13 (1998).
[23] I. A. Cunningham, ''Degradation of the detective quantum efficiency due to a nonunity detector fill factor,'' Proc. SPIE **3032**, 22–31 (1997).
[24] Y. El-Mohri, L. E. Antonuk, Q. Zhao, M. Maolinbay, X. Rong, K.-W. Jee, S. Nassif, and C. Cionca, ''A quantitative investigation of additive noise reduction for active matrix flat-panel imagers using compensation lines,'' Med. Phys. **27**, 1855–1864 (2000).